BULLETIN OF THE POLISH ACADEMY OF SCIENCES
TECHNICAL SCIENCES
DOI: 10.24425/bpasts.2026.1143

Investigation of Multilayer Tribological Coatings on CuSn10Pb10 Bronze Produced by Electrospark Alloying

Oksana HAPONOVA[1, 2*], Viacheslav TARELNYK[3], Nataliia TARELNYK[3], Gennadii LAPONOG[2], Stanislav SMOLENKO[2],Tomasz MOŚCICKI[1]

[1] Institute of Fundamental Technological Research Polish Academy of Sciences, Pawińskiego 5B, 02-106 Warsaw, Poland
[2] Sumy State University, Kharkivska 116, 40007, Sumy, Ukraine
[3] Sumy National Agrarian University, H. Kondratiieva 160, 40021 Sumy, Ukraine

Abstract. Bronzes are widely used as antifriction materials in sliding units. However, their performance depends heavily on the condition and structure of the surface layer. This study investigates the formation of multilayer antifriction coatings on CuSn10Pb10 bronze by electrospark alloying (ESA) using silver, lead, and tin electrodes. ESA was carried out in a sulphur-containing technological medium. Two technological schemes were implemented: conventional multilayer alloying (Ag → Pb → Ag and Ag → Sn → Ag) and alloying using a sulphur-containing medium ((S + Ag) → Pb → (S + Ag) and (S + Ag) → Sn → (S + Ag)). The microstructure, microhardness, surface roughness, and elemental distribution in the formed layers were investigated using optical microscopy, scanning electron microscopy with energy-dispersive analysis, and microhardness measurements. The tribological properties of the coatings were evaluated using a ball-on-disk configuration. It was determined that ESA produces a multilayer structure consisting of an outer layer, a bright sublayer, a heat-affected zone, and the substrate. The bright sublayer exhibited the highest microhardness values due to intensive material mixing and rapid melt solidification. The lowest friction coefficients (μ = 0.095–0.148) were obtained for sulphur-containing coatings. Introducing sulphur reduces the friction force by an average of 19%, due to a decrease in the adhesive component of friction and suppression of contact seizure.

Key words: electrospark alloying; sulphur-containing medium; bronze; multilayer coatings; tribological properties.

1. INTRODUCTION

Bronzes, particularly tin and aluminium bronzes, are traditionally used as materials for sliding components in mechanical engineering, aviation, hydraulics and power engineering due to their combination of a low friction coefficient, corrosion resistance and satisfactory wear resistance under moderate loads. However, recent review studies indicate that bronzes' performance characteristics are primarily determined by their microstructure, phase composition, and the mechanical properties of their surface layer [1]. The tribological behaviour of bronze is sensitive to structure, and controlling the microstructure of the surface layer is therefore a key factor in determining its wear resistance. Several studies have confirmed this relationship, demonstrating that modifying the bronze surface layer using thermal or other surface treatment methods influences the formation of a favourable structural–phase state on the surface, the stability of contact interaction, and the resistance to adhesive and abrasive wear [2–4].

In addition, theoretical and analytical studies of coated systems show that the mechanical response of functional coatings under local loading strongly depends on the gradient of material properties and the structural characteristics of the coating layer, which ultimately affect the stress–strain state and durability of tribological surfaces [5, 6].

According to H. Wei et. al., bronze coatings deposited by physical vapor deposition (PVD) exhibit higher wear resistance and a more stable friction coefficient (~0.1) compared with chemical vapor deposition (CVD) coatings and ductile cast iron in the cylinder block/valve plate tribological pair of an axial piston pump [7]. The improved performance is attributed to the optimal combination of hardness, the formation of Al–Cu intermetallic phases, and a more favourable surface layer microstructure, which determines the prevailing wear mechanisms.

Aluminium bronzes are widely used in marine and engineering applications due to their high corrosion resistance and satisfactory mechanical properties. Studies have shown that dense aluminium bronze coatings can be produced through low-pressure cold spray deposition followed by heat treatment. This process results in improved structural homogeneity and mechanical performance [8].

Copper-based alloys and their coatings remain among the primary antifriction materials for tribological applications. However, a main limitation of bronze friction pairs is their unstable running-in stage. During this stage, surface

roughness and geometric deviations reduce the real contact area. This leads to increased local stresses, temperature rise, and intensified adhesive wear and seizure. This issue persists even with modern bronze coatings, so optimizing the surface for improved running-in behaviour remains highly relevant.

The formation of functional coatings on bronze surfaces is considered a promising approach for improving wear resistance and facilitating the running-in conditions of friction pair components. Among the modern surface engineering methods employed to modify the near-surface layers of metallic materials, electrospark alloying (ESA) has attracted significant interest. This method is characterised by the high localisation of the energy of pulsed discharges, ensuring intensive mass transfer of the electrode material to the substrate surface and the formation of thin, strengthened layers with high adhesion. It also allows the structural and phase state to be controlled [9–11]. The combination of high technological efficiency, relatively low energy consumption and environmental friendliness is an important advantage of ESA, making it attractive for the restoration and strengthening of machine parts. Implementing this technology in industry enables the rapid restoration of the working surfaces of friction pair components and significantly extends their service life.

However, despite its advantages, ESA has certain limitations. The process efficiency strongly depends on the electro-physical properties of the electrode material, which must be electrically conductive to ensure stable discharge formation . This restricts the use of non-conductive or low-conductivity components that could enhance tribological performance. A promising approach to overcome this limitation is the use of special technological media (pastes or suspensions), which enable the introduction of additional components into the treatment zone regardless of their conductivity [12]. This expands the possibilities for controlling the composition and functional properties of coatings.

The formation of multicomponent coatings during ESA using powder materials introduced directly into the plasma of pulsed discharges was studied previously by V. Mihailov [13]. They also studied the formation of multicomponent coatings during ESA using powder materials introduced directly into the plasma of pulsed discharges. The authors implemented methods for supplying the powder material either through a hollow electrode or directly into the treatment zone, which significantly increased process productivity and intensified mass transfer onto the surface.

Further development of ESA technology involves optimising process parameters and coating compositions. According to [14], the formation of a two-layer coating on BrAZhMts 10-3-1.5 bronze is effective for creating wear-resistant regions based on Mn–Ni compounds, thereby improving the tribological characteristics of the material.

Compared with conventional surface modification methods, ESA is characterised by high adaptability to complex component geometries and the ability to perform local surface treatment without significant thermal deformation of the base material. In addition, the process does not require special gas environments or high-temperature technological operations [15, 16].

In addition, this technology enables a wide range of electrode materials to be used, opening up opportunities for the intentional control of the composition and properties of the resulting coatings. It has been shown in [17] that the use of a sulphur-containing paste in combination with a molybdenum electrode during ESA leads to the formation of a molybdenum disulfide (MoS_2) coating. Coatings obtained on a steel substrate demonstrated improved tribological properties, as confirmed by tribological test results. Therefore, using sulphur-containing technological media in ESA is a promising approach for modifying the surface of bronze components to improve running-in conditions and reduce friction. The application of ESA for the formation of multicomponent antifriction coatings on bronze alloys is a promising direction for improving their tribological performance.

Despite their widespread use, bronze sliding components often perform poorly during the initial running-in stage due to unstable contact conditions, increased adhesive interaction, and local overheating, all of which accelerate wear. Improving surface adaptability under these conditions is an important engineering challenge. From a scientific perspective, multilayer gradient coatings effectively control contact behavior and reduce wear. ESA enables the formation of strongly bonded surface layers; however, their tribological performance still needs improvement for severe friction conditions. From an application standpoint, enhanced bronze surfaces are highly relevant for sliding bearings in power engineering and hydraulic systems, where reliable operation, wear resistance, and repairability are critical.

This study aims to investigate the structure and properties of multilayer coatings formed by electrospark alloying on a bronze substrate using a sulphur-containing technological medium.

The scientific novelty of this work lies in a comprehensive study of the formation of multilayer anti-friction coatings on CuSn10Pb10 bronze using the electrospark alloying method with a sulphur-containing technological medium. Unlike previous studies, this work employs a combined approach that integrates multi-layer metallisation (Ag, Pb, Sn) with sulphur-containing paste, which has enabled the determination of the effect of sulphur on the microstructure, roughness and tribological characteristics of the coatings.

2. METHODOLOGY

CuSn10Pb10 bronze (UNI EN 1982) is a popular antifriction material for sliding bearing shells and liners. Its optimal combination of strength, wear resistance, and self-lubricating properties is due to the complex alloying of copper with tin and lead. The selection of CuSn10Pb10 bronze as the substrate material for this study is justified by its ability to withstand high specific loads and friction against hardened steel. These operating conditions are common in power engineering equipment with high rotational speeds and variable loading regimes where sliding bearings are widely used. The alloy's chemical composition is presented in Table 1.

For the experimental studies, 15 × 15 × 6 mm specimens were fabricated from cast CuSn10Pb10 bronze that was supplied without additional heat treatment and had a hardness of 1000-1200 MPa.

ESA of the bronze specimen surfaces was carried out using an "Elitron-22A" unit. Silver (Ag 99.9, EN 10093), lead (Pb 99.9, EN 12659), and tin (Sn 99.9, EN 610) electrodes, which were 4 mm in diameter and 20 mm in length, were used as anodes.

The coating formation process was implemented according to two technological schemes. According to the first scheme, the metals were sequentially deposited in the following orders: Ag → Pb → Ag and Ag → Sn → Ag. The discharge energy parameters for each stage were selected based on the values presented in Table 2. Figure 1 shows the processing scheme.

The second scheme involved forming modified layers using a special technological medium (STM). The STM was prepared as a viscous petroleum jelly emulsion containing 33.3 wt.% pure sulphur powder. Processing was performed according to the (S + Ag) → Pb → (S + Ag) and (S + Ag) → Sn → (S + Ag) sequences. The STM was applied to the working surface immediately before the silver deposition stage. To ensure the formed layer had low surface roughness parameters, the final silvering stage (third pass) was carried out at reduced discharge energy in the range of 0.05–0.36 J.

The ESA scheme according to the second technological approach is shown in Figure 2. ESA was performed using an Elitron-22A unit. During the ESA process, the following electrodes were used: silver (Ag 99.9, EN 10093), lead (Pb 99.9, EN 12659), and tin (Sn 99.9, EN 610). These electrodes were applied as 4 mm diameter, 20 mm long wires. The operating parameters of the equipment during ESA are presented in Table 3.

Surface roughness after ESA was measured using a profilograph-profilometer model 201 manufactured by the Kalibr plant. A MIM-7 optical microscope was used to perform metallographic analysis of the coatings. Microhardness measurements were carried out with a PMT-3 tester under a load of 20 g. Specimen preparation was conducted in accordance with standard procedures [18]. The distribution of chemical elements in the surface layer was investigated by scanning electron microscopy (SEM) using a REM-106 microscope equipped with a low-vacuum chamber and an energy-dispersive microanalysis system (EDS). Qualitative and quantitative analysis of local surface areas was performed using an XR-100FASTSDD detector.

The tribological properties of the coatings were evaluated using a T-01M tribometer in a ball-on-disc configuration (see Figure 3). The tests were performed using ring-shaped specimens (42 × 25 × 6 mm) made of CuSn10Pb10 bronze. The sulphur-containing STM was applied according to the second processing scheme (Figure 2). Additionally, an uncoated specimen was tested for comparison. A 6.3 mm diameter ball made of 100Cr6 steel was replaced after each test. Prior to each load increase, the specimens were lubricated with a drop of paraffin oil. During testing, the friction force (F) was continuously recorded. The operating parameters used were as follows: rotational speed ω = 353 rpm, linear sliding speed v = 0.67 m/s, sliding distance S = 300 mm, and applied load P = 1.0 kg (9.81 N).

3. RESULTS

3.1. Surface Roughness Evaluation

Analysis of the surface topography after ESA showed that microrelief characteristics were not significantly affected by the technological scheme. In all cases, the final stage involved silver electrode alloying at discharge energies of 0.05–0.36 J (Table 2).

As reported by T. Penyashki et. al., surface roughness parameters in ESA are primarily determined by discharge energy [19]. As discharge energy increases, local thermal impact intensifies, leading to melting of both the substrate and electrode materials. Consequently, deeper craters and a more developed microrelief structure form. During rapid cooling, some of the molten metal is ejected beyond the discharge zone while the rest solidifies into irregular deposits. This increases surface asperities and, consequently, roughness. It has been established that, following alloying at elevated energies, additional processing under mild conditions (low discharge energies) promotes the partial remelting of microrelief peaks and the filling of discharge craters. Consequently, a reduction in surface roughness is observed. Previous studies have also reported on the effectiveness of final treatment at reduced energy modes for roughness minimization.

Figure 3 shows the Rz values measured using different ESA technological schemes. The Rz values for all investigated treatments ranged from 7.5 to 10.0 µm for the Ag → Pb (Sn) → Ag schemes and from 5.5 to 7.5 µm for the S + Ag → Pb (Sn) → S + Ag schemes (see Table 4). Using the sulphur-containing STM reduces surface roughness parameters compared to conventional alloying schemes.

3.2. Microstructural Investigation

A metallographic analysis of coatings formed without the sulphur-containing STM according to the Ag → Pb → Ag and Ag → Sn → Ag schemes (first technological processing scheme, see Table 2) revealed that a multilayer structure consisting of an outer layer (OL), a bright sublayer (BS), a heat-affected zone (HAZ), and the substrate is formed in all cases (see Figure 4). The structure is clearly differentiated regardless of the second-layer material (Pb or Sn), while the thickness and microhardness depend on discharge energy and electrode composition.

The OL appears dark in metallographic cross-sections, is characterized by non-uniform thickness, and has relatively low microhardness (see Table 4). In the Ag → Pb → Ag system, the layer's thickness increases from 100–170 µm to 300–830 µm as discharge energy increases, while microhardness ranges from 80 to 140 MPa. When a tin electrode is used (Ag → Sn → Ag), the surface layer grows more intensely: its thickness reaches 2.0–2.7 mm, and its microhardness ranges from 130 to 183 MPa. The OL is continuous in all specimens. The formation of a massive surface layer is associated with repeated local melting and transfer of electrode material, followed by solidification in successive deposits. The more pronounced thickness increase in the case of tin may be attributed to more active diffusion interaction in the Cu–Sn system.

TABLE 1. Chemical composition of CuSn10Pb10 bronze according to BS EN 1982

Cu (+Ni)	Sn	Pb	Ni	Fe	Mn	Zn	Sb	P	S	Si	Al
78.0–82.0	9.0–11.0	8.0–11.0	≤2.000	≤0.250	≤0.200	≤2.000	≤0.500	≤0.100	≤0.100	≤0.010	≤0.010

TABLE 2. Technological regimes and energy parameters of electrospark alloying

	Specimens treated according to the regimes					
	1	2	3	4	5	6
Electrode sequence	Ag → Pb → Ag			Ag → Sn → Ag		
ESA discharge energy, W_p (J)	0.52; 0.13; 0.05	0.90; 0.36; 0.36	4.60; 4.60; 0.36	4.60; 0.36; 0.36	4.60; 0.90; 0.36	4.60; 4.60; 0.36
Electrode sequence	(S + Ag) → Pb → (S + Ag)			(S + Ag) → Sn → (S + Ag)		
ESA discharge energy, W_p (J)	0.52; 0.13; 0.05	0.90; 0.36; 0.36	4.60; 4.60; 0.36	4.60; 0.36; 0.36	4.60; 0.90; 0.36	4.60; 4.60; 0.36

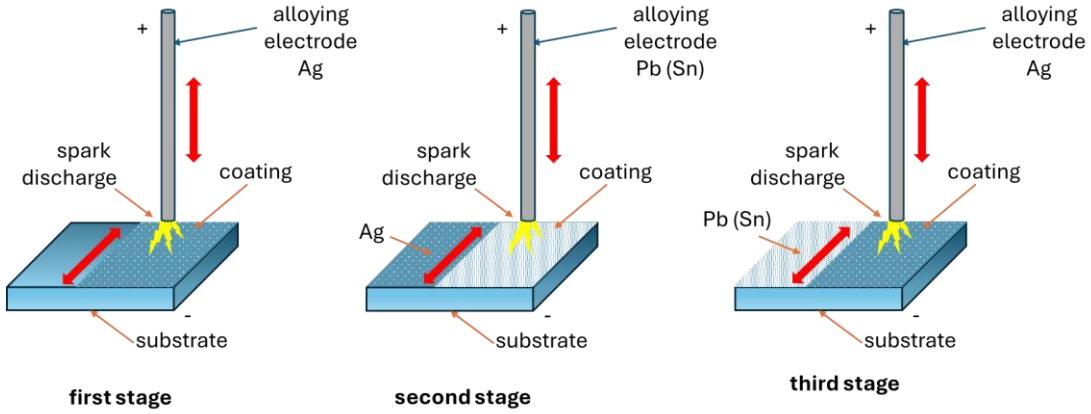

Fig.1. Specimen processing scheme according to the first scheme: Ag → Pb → Ag and Ag → Sn → Ag.

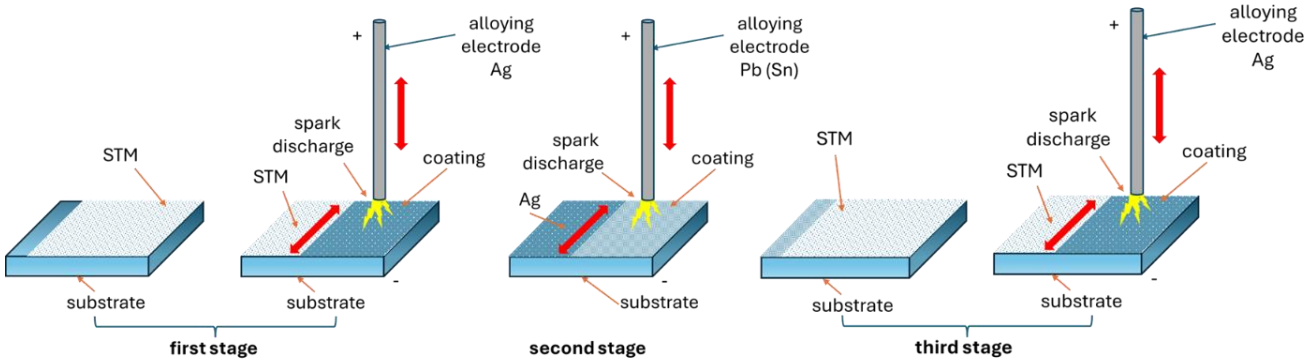

Fig.2. Specimen processing scheme according to the second scheme: (S + Ag) → Pb → (S + Ag), or (S + Ag) → Sn → (S + Ag).

TABLE 3. Operating parameters of the Elitron 52-A unit

Type of generator	Capacitance, C, μF	Voltage, U, V	Pulse duration, s	Discharge energy, W_p, J	Productivity, cm^2/min
Transistor–thyristor (TT)	120	35	$10^{-7} – 10^{-8}$	0.05	1.0 – 1.3
		75		0.13	
		100		0.36	
	300	75		0.52	
		100		0.90	

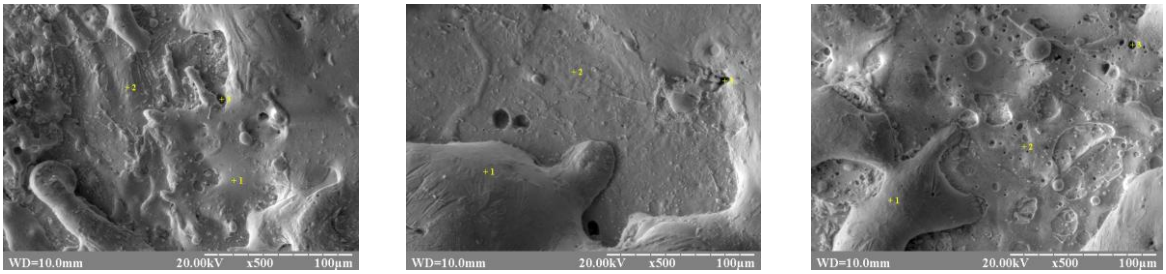

a b c

Fig.3. Coating morphology of samples after ESA according to the second scheme S + Ag → Pb → S + Ag: a - Sample 1, b - Sample 2, c - Sample 3. See Table 2 for regimes.

TABLE 4. Parameters of the obtained coatings

Specimens*	OL thickness, µm	OL microhardness, MPa	OL continuity, %	BS thickness, µm	BS microhardness, MPa	BS continuity, %	Surface roughness, Rz, µm	Hardened layer thickness, µm	Hardened layer microhardness, MPa
Ag → Pb → Ag									
1	100–170	81–91	100	up to 10	–	50–60	8.5	80	1494–2230
2	150–250	90–140	100	up to 10	912	70–80	7.5	165	1382–2118
3	300–830	80–100	100	30–40	1150–858	70–80	7.5–10.0	230	1556–1845
Ag → Sn → Ag									
4	530–670	183	100	10–25	1228	100	8.5–10.0	70	1313–1525
5	700–1750	134	100	10–25	1616	100	8.5–10.0	90	1467–1636
6	2030–2740	130–154	100	10–25	2383	100	8.5–10.0	120	1550–2383
S + Ag → Pb → S + Ag									
1	60–90	80–90	100	up to 10	1030	70–80	6.5	60	1400–2250
2	80–100	90–130	100	up to 10	1100	70–90	5.5	115	1400–2250
3	210–300	80–110	100	20–40	1150–900	70–90	7.5	130	1500–1900
S + Ag → Sn → S + Ag									
4	530–670	140	100	10–20	1250	100	6.5–7.5	60	1300–1500
5	700–1750	150	100	10–30	1730	100	6.5–7.5	90	1457–1685
6	2030–2740	130–150	100	10–30	2270	100	6.5–7.5	110	1650–2410

* The specimens were treated according to the regimes in Table 2.

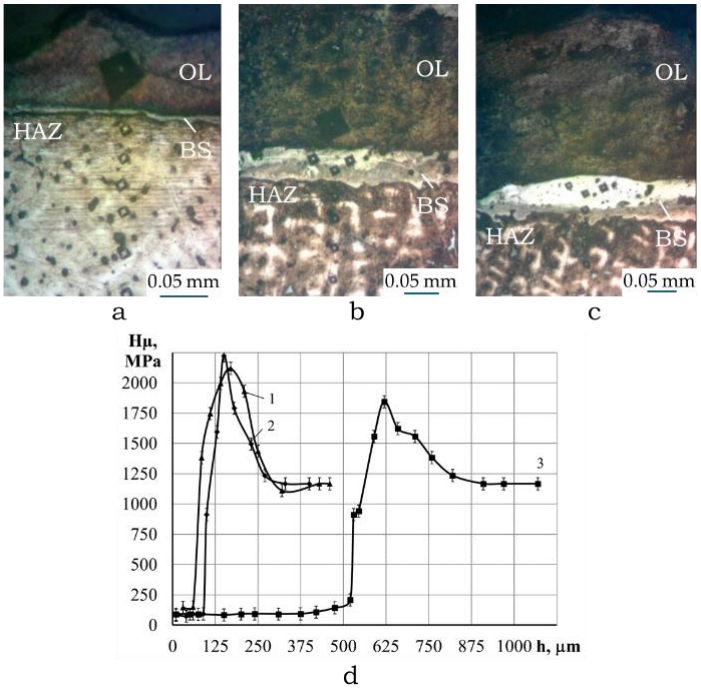

Fig.4. Microstructures of coatings formed according to the Ag → Pb → Ag scheme: a–c – specimens 1–3, respectively; d – microhardness distribution across the coating thickness (curves 1–3 correspond to specimens 1–3 processed under the regimes given in Table 2). In (a–c): OL – outer layer; BS – bright sublayer; HAZ – heat-affected zone.

HAZ is observed below the BS. The thickness of the HAZ increases with discharge energy and ranges from 80 to 230 μm for Pb-containing coatings and from 70 to 120 μm for Sn-containing coatings. The microhardness of this zone (1313–2383 MPa) is greater than that of the substrate (approximately 1235 MPa), suggesting structural changes in the bronze resulting from pulsed heating and rapid cooling. Dispersion strengthening of the α-solid solution and partial redistribution of eutectoid constituents are likely occurring.

A metallographic analysis of coatings formed with a preliminary application of sulphur-containing STM, according to the S + Ag → Pb → S + Ag and S + Ag → Sn → S + Ag schemes, revealed that the general multilayer architecture remains intact.

This structure consists of an outer layer (OL), a bright sublayer (BS), a heat-affected zone (HAZ), and the substrate. Compared to coatings produced without sulfidation, the thickness of the OL is generally lower under identical alloying regimes: 60–300 μm for Pb-containing systems and 530–2740 μm for Sn-containing systems. The increase in thickness with discharge energy is less pronounced. This may be related to changes in the electrophysical discharge conditions caused by the preliminary application of the sulphur-containing STM, which affects heat generation and mass transfer efficiency in the treatment zone. The BS is present in all specimens (thickness: 10–40 μm), with microhardness values of 900–1150 MPa for Pb-containing coatings and 1250–2270 MPa for Sn-containing coatings. This sublayer forms from the intensive mixing of the electrode material with the substrate during pulsed melting.

Analysis of the distribution of elements in surface layers showed that, during ESA and the use of a sulphur-containing STM, there is noticeable diffusion of electrode metals (Pb, Sn, and Ag) into the bronze substrate, as well as limited penetration of sulphur into the coating. For Pb-containing coatings, the depth of the sulphur diffusion zone increases from 90 to 200 μm with rising discharge energy, while the depth of the zone for silver reaches up to 225 μm. These results indicate the intensive mixing of the electrode materials and STM and their diffusion into the substrate. A similar trend is observed in Sn-containing coatings, with an increase in coating thickness and expansion of the sulphur diffusion zone up to 200 μm.

As discharge energy increases, the diffusion zone expands due to intensified thermal effects. This indicates that electrospark alloying involves simultaneous remelting, mass transfer, and diffusion, leading to the formation of a multilayer structure with improved coating adhesion.

3.3. Tribological Investigation

To evaluate the tribological performance of the coatings, ball-on-disc tests were performed. The evolution of the friction force for specimens processed under the regimes listed in Table 2 is shown in Figure 5, while the average friction forces (F) and the corresponding coefficients of friction (μ) are given in Table 5.

Analysis of the results revealed that the friction force of the uncoated sample (No 0) gradually increased throughout the entire testing period (Fig. 5a). This wear behavior indicates an increase in contact area due to plastic deformation of the bronze surface and increasing adhesive interaction with the steel ball. The absence of a stabilization region suggests that the running-in stage was not fully completed, meaning a stable tribolayer did not form. This leads to intensive wear.

For sample 1, which has a coating thickness of 0.19 mm and an Rz roughness of 7.5 μm, the friction force initially increases and stabilizes at a constant level after a sliding distance of approximately 200 m. Stabilization of the friction force after the running-in stage indicates the formation of a stable tribolayer and a transition to a steady wear regime.

Increasing the coating thickness of samples 2 and 3 to 0.26 and 1.01 mm, respectively, with a roughness of 8.5–10.0 μm (Rz), is accompanied by an increase in friction force and fluctuations in the friction curve. This reflects the running-in process of the surface (Fig. 5b). Initial friction fluctuations are caused by contact instability due to surface roughness and structural inhomogeneity. During this period, there is local shearing of micro-asperities, partial destruction of the surface layer, and redistribution of material in the contact zone. A decrease in the amplitude of the fluctuations, as well as the gradual stabilization of the friction force during testing, indicates that the running-in stage has been completed and a more stable contact state has formed.

For samples with maximum coating thicknesses (No 4–6; S + Ag → Pb → S + Ag, and S + Ag → Sn → S + Ag), there is a slight increase in friction force at the beginning of the tests, followed by stabilization at 0.9–2.2 N (Fig. 5c).

According to Table 5, samples 4 and 1 recorded the lowest coefficient of friction values (0.095 and 0.148, respectively), while samples 3 and 6 recorded the highest values (0.259 and 0.219, respectively). A comparison of the results shows that samples with sulphur-containing coatings exhibit lower friction forces and coefficients of friction than similar coatings without sulphur (sample 7). This indicates the positive effect of sulfidation in reducing the adhesive component of friction and decreasing the intensity of contact adhesion between surfaces.

On average, introducing sulphur into the STM composition reduces the friction force of a steel ball on bronze sample surfaces by approximately 19%, compared to coatings without sulphur. The most effective coatings are formed according to the S + Ag → Pb → S + Ag and S + Ag → Sn → S + Ag schemes, with discharge energies of 0.52 → 0.13 → 0.05 J and 4.6 → 0.36 → 0.36 J, respectively (see Table 2). Under these conditions, the friction force decreases by a factor of 1.90 and 1.22, respectively, compared to the uncoated sample. The results confirm that the proposed technology for applying sulphur-containing STM multilayer coatings using the ESA method allows for the formation of sufficiently thick coatings (0.19–1.31 mm) for subsequent mechanical processing, significantly improving the tribological characteristics of bronze parts. This improvement is due to a reduction in friction force, limitation of adhesive interactions, and stabilization of the contact surface during operation.

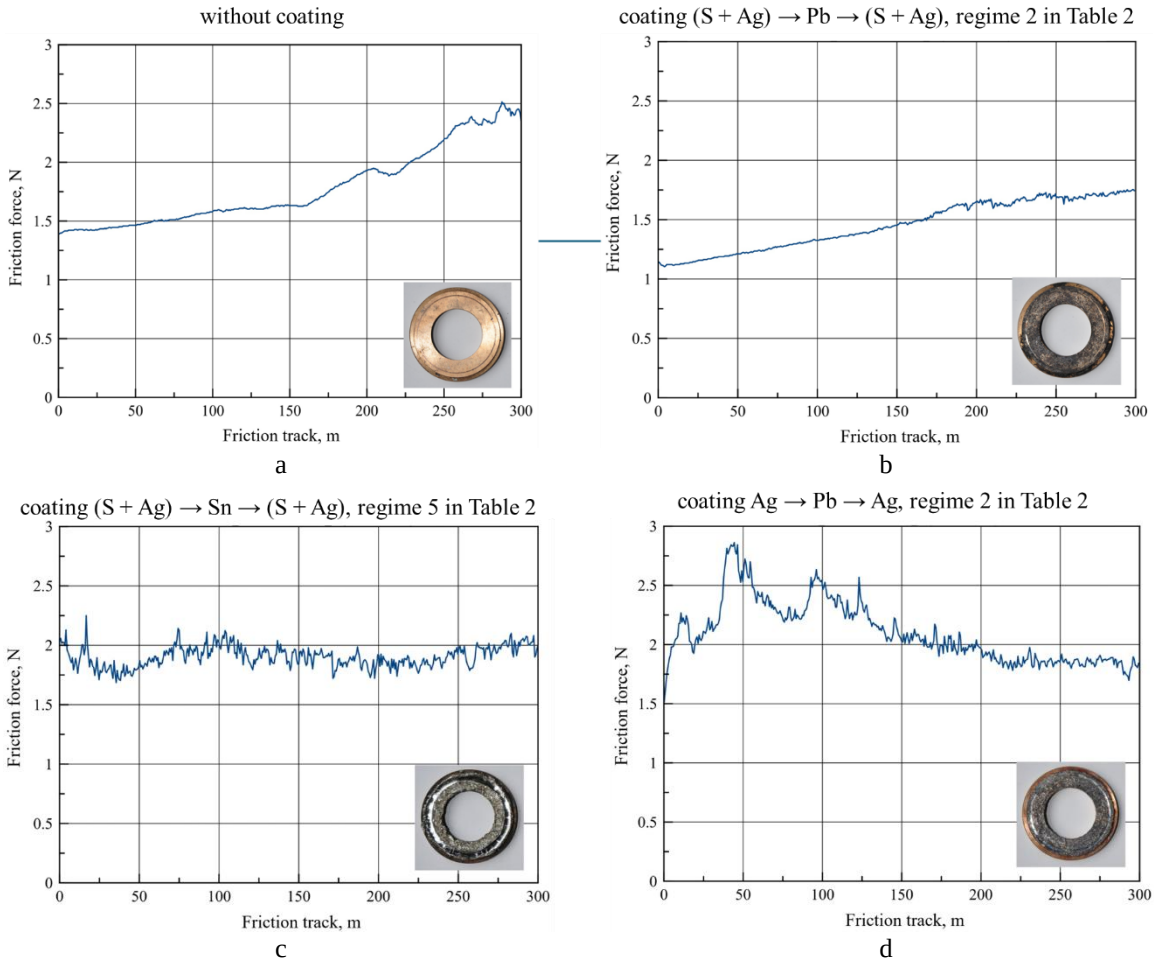

Fig.5. Evolution of the friction force of a steel ball sliding against ESA-treated specimens: a – uncoated specimen; b – coating (S + Ag) → Pb → (S + Ag) (specimen 2 regime, Table 2); c – coating (S + Ag) → Sn → (S + Ag) (specimen 5 regime, Table 2); d – coating Ag → Pb → Ag (specimen 2 regime, Table 2).

TABLE 5. Friction force and coefficient of friction of a steel ball on the surface of a bronze disc with coating.

Specimen*	Treatment scheme	Friction force, F (N)	Coefficient of friction, μ
0	Without coating (CuSn10Pb10 bronze)	1.779	0.181
1	S + Ag → Pb → S + Ag	1.454	0.148
2	S + Ag → Pb → S + Ag	1.762	0.179
3	S + Ag → Pb → S + Ag	2.543	0.259
4	S + Ag → Sn → S + Ag	0.934	0.095
5	S + Ag → Sn → S + Ag	1.904	0.194
6	S + Ag → Sn → S + Ag	2.152	0.219
7**	Ag → Pb → Ag	2.098	0.214

* The specimens were treated according to the regimes in Table 2.
** The specimen was treated under regime 2 according to Table 2.

The results can be explained by the role of individual coating layers and their formation features. The outer layer (OL), which has relatively low microhardness, promotes surface adaptation during the running-in stage and reduces local contact stresses. The bright sublayer (BS) exhibits the highest microhardness and performs a load-bearing function, largely determining the wear resistance of the coating system. The heat-affected zone (HAZ) ensures a gradual transition of mechanical properties to the substrate, improving adhesion of the coating and its resistance to delamination under loading. This gradient of properties is an important factor in stable tribological behaviour. Concurrently, the reduction in the coefficient of friction for sulfur-containing coatings is attributed to a decrease in adhesive interaction and the formation of thin tribochemical films with low shear strength on the contact surface [20, 21]. These films act as solid lubricating layers that stabilize friction and reduce seizure tendencies.

4. CONCLUSIONS

1. Improving the wear resistance and reducing the friction of CuSn10Pb10 bronze bearings is crucial for friction components in power equipment that operate under high loads and speeds. Electrospark alloying (ESA) is a promising method for modifying the surface layer to form functional antifriction coatings without altering the material's bulk properties.
2. A technology for forming multilayer coatings using the ESA method has been proposed, particularly with the use of a special technological medium (STM) containing sulphur. Using STM enables the regulation of mass transfer and thermal processes in the discharge zone, the control of the outer layer's thickness while maintaining the hardened sublayer's high microhardness, and the assurance of 100% coating continuity. An additional advantage is the ability to form layers up to 1.3 mm thick, simplifying the mechanical processing of finished products.
3. It was determined that surface roughness parameters are primarily influenced by discharge energy in the final stage of treatment. Conventional processing schemes result in Rz values ranging from 7.5 to 10.0 μm. The use of STM, however, reduces roughness to 5.5–7.5 μm.
4. Metallographic studies revealed that all processing variants result in a multilayer structure comprising an outer layer, a bright subsurface layer, a heat-affected zone, and the substrate. The outer layer has relatively low microhardness and acts as an antifriction layer during the initial use period. The bright subsurface layer exhibits the highest microhardness values (up to 2383 MPa for Sn-containing coatings) due to the intensive mixing of the electrode material with the substrate and the rapid solidification of the melt. This layer determines the coating's load-bearing capacity and wear resistance.
5. Tribological tests showed that the friction behaviour of the coated sample was more stable than that of the uncoated sample. The lowest coefficients of friction ($\mu = 0.095–0.148$) were obtained with sulphur-containing coatings. Adding sulphur to the STM reduced the friction force by an average of 19%, due to a decrease in the adhesive component of friction and limited contact adhesion. The most effective coatings are S + Ag → Pb → S + Ag and S + Ag → Sn → S + Ag.
6. ESA technology using STM containing sulphur is recommended for modifying bearing bronze surfaces operating under dry or boundary lubrication conditions. Using optimized processing regimes enables the formation of thick, continuous, and tribologically effective coatings.
7. Further research should include phase analysis of the formed coatings, detailed wear characterization, and statistical validation of the results to provide a deeper understanding of the mechanisms governing tribological behavior and to optimize processing parameters.

ACKNOWLEDGEMENTS

The authors are grateful to Vasyl Martsynkovskyy, PhD, Director of TRIZ Ltd., for support in implementing the proposed technology under industrial conditions. The authors also acknowledge the support of the Ministry of Education and Science of Ukraine within the framework of research project No. 0124U000539, and the National Research Foundation of Ukraine under project No. 2025.07/0115.

STATEMENT AND DECLARATIONS

Data availability statement: All data used in this research appear in the submitted article.
Conflicts of interest: The authors declare that there is no conflict of interest.

REFERENCES

[1] R. D. Chauhan and P. K. Bharti, "A review of tribological excellence of bronze alloys," *Discov. Appl. Sci*., vol. 7, 283, 2025, doi: 10.1007/s42452-025-06610-4.
[2] Y. Du, Y. Dong, S. Ma, X. Yang, J. Ju, Z. Shen, Z. Suo, L. Fu, and A. Shan, "Insight into the tribological behavior of the dual-phase nickel aluminum bronze alloy by multiscale characterization," *Wear*, vol. 556–557, 2024, 205530, doi: 10.1016/j.wear.2024.205530.
[3] J. Pan, J. Yin, Y. Xia, D. Yao, H. Liang, K. Zuo, and Y. Zeng, "The microstructure and properties of bronze matrix composites with surface-modified graphite by titanium carbide adhesion," *Tribol. Int*., vol. 140, 2019, 105892, doi: 10.1016/j.triboint.2019.105892.
[4] ASM Handbook, Vol. 18: Friction, *Lubrication, and Wear Technology*, ASM International, 2017.
[5] I. Shatskyi, M. Makoviichuk, L. Ropyak, and A. Velychkovych, "Analytical Model of Deformation of a Functionally Graded Ceramic Coating under Local Load," *Ceramics*, vol. 6, pp. 1879–1893, 2023, doi: 10.3390/ceramics6030115.
[6] V. B. Tarelnyk, O. P. Gaponova, Ye. V. Konoplianchenko, V. S. Martsynkovskyy, N. V. Tarelnyk, and O. O. Vasylenko, "Improvement of Quality of the Surface Electroerosive Alloyed Layers by the Combined Coatings and the Surface Plastic Deformation. III. The Influence of the Main Technological Parameters on Microgeometry, Structure and Properties of Electrolytic Erosion Coatings," *Metallofiz. Noveishie Tekhnol*., vol. 41, no. 3, pp. 313–335, 2019, doi: 10.15407/mfint.41.03.0313.
[7] H. Wei, L. Larbi, H. Dong, D. Wang, and S. Li, "A comparative investigation on wear behaviors of physical and chemical vapor deposited bronze coatings for hydraulic piston pump," *Chin. J. Aeronaut.*, vol. 37, no. 3, pp. 391–403, 2024, doi: 10.1016/j.cja.2024.01.004.
[8] M. Winnicki, A. Baszczuk, A. Gibas, and M. Jasiorski, "Experimental study on aluminium bronze coatings fabricated by low pressure cold spraying and subsequent heat treatment," *Surf. Coat. Technol*., vol. 456, 129260, 2023, doi: 10.1016/j.surfcoat.2023.129260.
[9] V. B. Tarelnyk, Ie. V. Konoplianchenko, O. P. Gaponova, N. V. Tarelnyk, V. S. Martsynkovskyy, B. O. Sarzhanov, O. A. Sarzhanov,

and B. Antoszewski, “Effect of Laser Processing on the Qualitative Parameters of Protective Abrasion-Resistant Coatings,” *Powder Metall. Met. Ceram.*, vol. 58, pp. 703–713, 2020, doi: 10.1007/s11106-020-00127-8.

[10] O. P. Umanskyi, M. S. Storozhenko, V. B. Tarelnyk, O. Yu. Koval, Yu. V. Gubin, N. V. Tarelnyk, and T. V. Kurinna, “Electrospark Deposition of FeNiCrBSiC–MeB2 Coatings on Steel,” *Powder Metall. Met. Ceram.*, vol. 59, pp. 57–67, 2020, doi: 10.1007/s11106-020-00138-5.

[11] J. Yan, R. Abbasi, X. Zhao, P. Peng, and N. Y. Zhou, “Electrospark-Deposited AlCrFeCoNi High-Entropy Alloy Coatings on Steel: Microstructure Evolution, Mechanical Properties, and Corrosion Response,” *Adv. Eng. Mater.*, vol. 28, e202501186, 2025, doi: 10.1002/adem.202501186.

[12] O. P. Gaponova, B. Antoszewski, V. B. Tarelnyk, P. Kurp, O. M. Myslyvchenko, and N. V. Tarelnyk, “Analysis of the Quality of Sulfomolybdenum Coatings Obtained by Electrospark Alloying Methods,” *Materials*, vol. 14, 6332, 2021, doi: 10.3390/ma14216332.

[13] V. Mihailov, N. Kazak, S. Ivashcu, E. Ovchinnikov, C. Baciu, A. Ianachevici, R. Rukuiza, and A. Zunda, “Synthesis of Multicomponent Coatings by Electrospark Alloying with Powder Materials,” *Coatings*, vol. 13, no. 3, 651, 2023, doi: 10.3390/coatings13030651.

[14] E. Solovykh, I. Shepelenko, M. Chernovol, S. Mahopets, A. Solovuch, and S. Katerynych, “Optimization of the technology for applying discrete coatings in restoration of bronze parts by electrospark alloying,” *Problems Tribol.*, vol. 28, no. 1/107, pp. 51–58, 2023, doi: 10.31891/2079-1372-2023-107-1-51-58.

[15] O. Melnyk, O. Onishchenko, S. Kurdiuk, M. Bulgakov, O. Fomin, V. Píštěk, and P. Kučera, “Pulse-Driven Surface Hardening and Advanced Electrospark Alloying for Maritime Applications,” *J. Mar. Sci. Eng.*, vol. 13, no. 9, 1624, 2025, doi: 10.3390/jmse13091624.

[16] O. Deviatko, M. Denisenko, N. Kanivets, and M. Tuziuk, "Electric Spark Alloying is an Effective Method of Surface Hardening of Metal Materials," in *Advanced Manufacturing Processes VII*, V. Tonkonogyi, V. Ivanov, S. Luściński, J. Trojanowska, and G. Oborskyi, Eds., Cham: Springer, 2026, Lecture Notes in Mechanical Engineering, doi: 10.1007/978-3-032-14926-8_35.

[17] O. P. Gaponova, V. B. Tarelnyk, B. Antoszewski, N. Radek, N. V. Tarelnyk, P. Kurp, O. M. Myslyvchenko, and J. Hoffman, “Technological Features for Controlling Steel Part Quality Parameters by the Method of Electrospark Alloying Using Carburezer Containing Nitrogen–Carbon Components,” *Materials*, vol. 15, 6085, 2022, doi: 10.3390/ma15176085.

[18] R. N. Caron, R. G. Barth, and D. E. Tyler, “Metallography and Microstructures of Copper and Its Alloys,” in *Metallography and Microstructures*, vol. 9, *ASM Handbook*, ASM International, 2004, pp. 775–788.

[19] T. Penyashki, G. Kostadinov, M. Kandeva, A. Nikolov, R. Dimitrova, V. Kamburov, P. Danailov, and S. Bozhkov, “Study of the Influence of Coating Roughness on the Properties and Wear Resistance of Electrospark Deposited Ti6Al4V Titanium Alloy,” *Tribol. Ind.*, vol. 46, no. 1, pp. 13–28, 2024, doi: 10.24874/ti.1508.06.23.08.

[20] J. Jin, Y. Yang, and T. Ma, “Study on tribological properties of Ag–MoS_2 self-lubricating films,” *Surf. Coat. Technol.*, vol. 503, Art. no. 132003, 2025, doi: 10.1016/j.surfcoat.2025.132003.

[21] O. Haponova, V. Tarelnyk, T. Mościcki, N. Tarelnyk, J. Półrolniczak, O. Myslyvchenko, B. Adamczyk-Cieślak, and J. Sulej-Chojnacka, “Investigation of the Structure and Properties of MoS_2 Coatings Obtained by Electrospark Alloying,” *Coatings*, vol. 14, 563, 2024, doi: 10.3390/coatings14050563.